Letters

Analysis and Control of Three-Phase Modular Multilevel Converters Under the Single Arm Fault Condition

Chao Wang, *Student Member, IEEE*, Kui Wang, *Senior Member, IEEE*, Zedong Zheng, *Senior Member, IEEE*, Bo Yang, *Member, IEEE*, Kai Sun, *Senior Member, IEEE*, and Yongdong Li, *Member, IEEE*

***Abstract*—Modular multilevel converter (MMC) is an attractive topology for medium- and high-voltage applications due to the merits of high modularity, easy scalability, high-quality output voltage, and fault tolerance of submodules. This letter focuses on the control of a three-phase MMC under the single arm fault condition, which can further improve the fault tolerance ability of the MMC. According to three essential operating constraints of the MMC, this letter proposes a feasible arm voltage and current configuration method for the single arm failed MMC, which can guarantee its stable operation with reduced output power. Several operating limitations are also discussed. Experiment results based on a prototype with four half-bridge submodules per arm are presented to verify the proposed arm fault tolerance method.**

***Index Terms*—Arm voltage and current configuration, energy balance, modular multilevel converter (MMC), operating limitations, single arm fault.**

I. Introduction

SINCE the modular multilevel converter (MMC) has been proposed in 2003 [1], it has caught great attention of industry and academia in the past decade [2], due to its attractive advantages in medium- and high-voltage (HV) applications, such as HV direct current transmission, medium-voltage (MV) motor drives, and power electronics transformers. As it is generally employed in MV and HV applications, reliability is of great importance. Fortunately, the MMC is convenient to configure redundant submodules (SMs) to guarantee its safe operation under SM failure conditions, since it is a kind of modular cascaded topology. To implement the fault tolerance control under this condition, several effective methods about SM open-circuit detection [3], [4] and smooth fault tolerant control [4]–[6] have been proposed.

Manuscript received January 15, 2019; accepted March 17, 2019. Date of publication March 24, 2019; date of current version June 10, 2019. This work was supported by the National Natural Science Foundation of China under Grant 51777110. *(Corresponding author: Zedong Zheng.)*

C. Wang, K. Wang, Z. Zheng, K. Sun, and Y. Li are with the Department of Electrical Engineering, State Key Laboratory of Power System, Tsinghua University, Beijing 100084, China (e-mail:

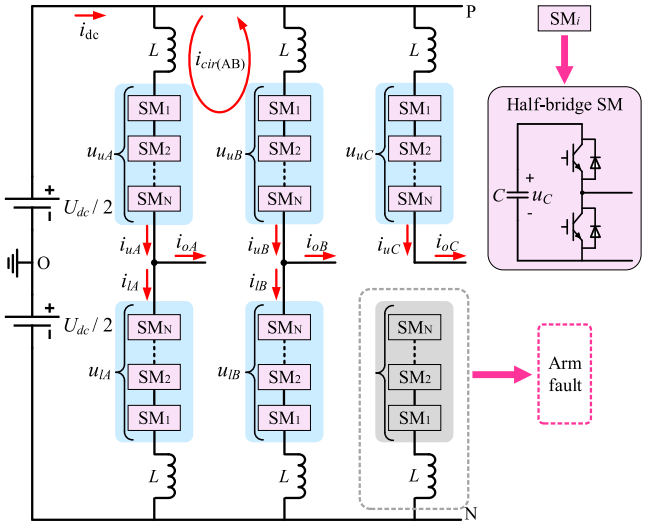

Fig. 1. Circuit configuration of the MMC when the lower arm of phase C is failed.

fault conditions, it is also desired that the MMC can still operate steadily under the SAF condition. Therefore, the following three primary constraints must be satisfied.

"Constraint 1": The output currents should be maintained as desired, which is equivalent to maintaining the line voltages as desired for a three-phase balanced system.

"Constraint 2": The total energy of each arm should be controlled balanced, which is equivalent to that the dc power of each arm should be 0.

"Constraint 3": The dc-link current, $i_{\rm dc}$, does not contain fundamental current component (FCC).

The first two constraints are essential control objectives of the MMC, and the last one is a derived requirement for a three-phase symmetrical MMC operating under the normal condition.

A. Arm Voltage Configuration

The output phase voltages and currents of the three-phase MMC under the normal condition can be written as (1), where φ is the power factor angle and x refers to A, B, and C

$$\begin{cases} u_{oX} = U_o \cos(\omega_o t + \theta_X),\ i_{oX} = I_o \cos(\omega_o t - \varphi + \theta_X) \\ \theta_A = 0,\ \theta_B = -2\pi/3,\ \theta_C = 2\pi/3. \end{cases} \tag{1}$$

When the lower arm of phase C malfunctions and is removed from the system, it is evident that the whole output current of phase C flows through the upper arm of phase C, that is

$$i_{uC} = i_{oC} = I_o \cos(\omega_o t + 2\pi/3 - \varphi). \tag{2}$$

As a result, there is no control degree of freedom for i_{uC} anymore. According to "Constraint 2," p_{uC}, which is defined as (3), should not contain the dc component

$$p_{uC} = u_{uC} i_{uC}. \tag{3}$$

Thus, considering the orthogonality of sine function, u_{uC} should not contain the fundamental voltage component (FVC), unless the phase angle difference between it and i_{uC} is $\pm\pi/2$. Otherwise, the dc component occurs in p_{uC} and the energy of this arm diverges. According to the symmetrical characteristics of the MMC, u_{uC} should be configured as (4), in which only the dc component and a common-mode component $u_{\rm com}$ are included. It should be noted that $u_{\rm com}$ can be any waveform as long as it does not include any fundamental component

$$u_{uC} = U_{\rm dc}/2 - u_{\rm com}. \tag{4}$$

Then, it is easy to derive that the arm voltages of phase A and B should be configured as (5) to satisfy "Constraint 1." Since FVCs in phase A and B are $u_{AC} = u_{oA} - u_{oC}$ and $u_{BC} = u_{oB} - u_{oC}$, the third-order harmonic injection cannot increase the MMI, i.e., $m_{\max}$, considering that the phase difference between u_{AC} and u_{BC} is $\pi/3$. From this point of view, the best choice is to set $u_{\rm com} = 0$

$$\begin{cases} u_{uA} = U_{\rm dc}/2 - (u_{oA} - u_{oC}) - u_{\rm com} \\ u_{lA} = U_{\rm dc}/2 + (u_{oA} - u_{oC}) + u_{\rm com} \\ u_{uB} = U_{\rm dc}/2 - (u_{oB} - u_{oC}) - u_{\rm com} \\ u_{lB} = U_{\rm dc}/2 + (u_{oB} - u_{oC}) + u_{\rm com}. \end{cases} \tag{5}$$

B. Arm Current Configuration

Since $i_{uC} = i_{oC}$, i_{oC} needs to be injected into the arms of phase A and B to counteract i_{uC} to guarantee "Constraint 3." Assuming all even-order circulating currents are suppressed, the arm currents of phase A and phase B can be expressed as (6), where $I_{{\rm cir}X,0}$ refers to dc circulating current and $i_{\rm cir(AB)}$ refers to the circulating current between phase A and B (as shown in Fig. 1). x_X and y_X are undetermined coefficients which need to be solved by the aforementioned constraints

$$\begin{cases} i_{uA} = x_A i_{oA} + y_A i_{oC} + I_{{\rm cir}A,0} + i_{\rm cir(AB)} \\ i_{lA} = (x_A - 1) i_{oA} + y_A i_{oC} + I_{{\rm cir}A,0} + i_{\rm cir(AB)} \\ i_{uB} = x_B i_{oB} + y_B i_{oC} + I_{{\rm cir}B,0} - i_{\rm cir(AB)} \\ i_{lB} = (x_B - 1) i_{oB} + y_B i_{oC} + I_{{\rm cir}B,0} - i_{\rm cir(AB)}. \end{cases} \tag{6}$$

The KCL equations of node P and node N can be written as follows:

$$i_{uA} + i_{uB} + i_{uC} = i_{\rm dc} = i_{lA} + i_{lB}. \tag{7}$$

According to "Constraint 3," there is no FCC in $i_{\rm dc}$, thus (8) is derived by summing FCCs in all upper or lower arms

$$x_A i_{oA} + x_B i_{oB} + (y_A + y_B) i_{oC} + i_{oC} = 0. \tag{8}$$

For three-phase loads with star connection, $i_{oC} = -(i_{oA} + i_{oB})$. Thus, it can be derived that the following relationships exist:

$$x_A = x_B = x, \quad y_A + y_B = (x - 1). \tag{9}$$

The relationship between y_A and y_B can be rewritten as follows:

$$y_A = (x - 1)/2 + k, \quad y_B = (x - 1)/2 - k. \tag{10}$$

Assuming $i_{\rm cir(AB)} = 0$, the dc power component of each arm, $p_{uX,0}$ and $p_{lX,0}$, can be calculated by multiplying the corresponding equations in (5) and (6), which should be 0 according to "Constraint 2." $p_{uX,0}$ and $p_{lX,0}$ are easy to be acquired by calculating the projections of currents in voltage directions,

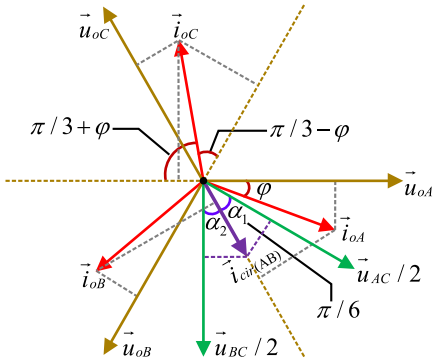

Fig. 2. Phasor diagram for dc power analysis.

according to the phasor diagram shown in Fig. 2. But it is challenging to acquire feasible x and k by directly solving separate dc power equations because each equation is related to two variables. However, similar to the normal condition of the MMC, the energy balance of each arm is equivalent to the common mode (CM) and differential mode (DM) energy balance of the upper and lower arm. Thus, separate dc power equations are identical to (11), shown as bottom of this page, which consist of CM power equations (CMPEs, the first two) and DM power equations (DMPEs, the last two).

On one hand, for CMPEs, it is evident that they can be controlled to 0 as long as $I_{\mathrm{cir}A,0}$ and $I_{\mathrm{cir}B,0}$ are controlled to desired values. On the other hand, for any given φ, it can be proved that there are available solutions $x(\varphi)$ and $k(\varphi)$ to make DMPEs tenable. However, their values are functions of φ, which means it is required to calculate φ and solve DMPEs to obtain $x(\varphi)$ and $k(\varphi)$ in real time for different load conditions, leading to the increment of computational efforts. What is more, the closed-loop control is also necessary to adjust $x(\varphi)$ and $k(\varphi)$, considering the parametric errors of actual systems. Since $x(\varphi)$ and $k(\varphi)$ are related to two equations at the same time, the closed-loop control may be quite complex. Therefore, this is not the best solution

If x and k are always equal to 0, DMPEs can be rewritten as follows:

$$\begin{aligned} p_{uA,0}-p_{lA,0}|_{x=k\equiv 0} &= -\left(p_{uB,0}-p_{lB,0}|_{x=k\equiv 0}\right) \\ &= \sqrt{3}U_oI_o\sin\varphi/2. \end{aligned} \tag{12}$$

Although DMPEs are not 0, they are opposite to each other under this condition. Therefore, if the additional dc power expressed by (13) is injected in each arm, DMPEs can be controlled to 0 and "Constraint 2" is satisfied

$$\Delta p_{uA,0}=-\Delta p_{lA,0}=-\Delta p_{uB,0}=\Delta p_{lB,0}=-\sqrt{3}U_oI_o\sin\varphi/4. \tag{13}$$

To produce such additional dc power, a proper control degree of freedom should be selected at first. Since arm voltages, x, and k are determined, $i_{\mathrm{cir(AB)}}$ which is assumed to be 0 aforementioned is a proper one. According to the orthogonality of sine function and (5), the dc power can be produced when $i_{\mathrm{cir(AB)}}$ contains the FCC. Then, the final task is to calculate the phase angle and amplitude of $i_{\mathrm{cir(AB)}}$.

The FVCs in arms of phase A and B are u_{AC} and u_{BC}, with amplitude equaling to $\sqrt{3}U_o$. Assuming the amplitude of $i_{\mathrm{cir(AB)}}$ is $I_{\mathrm{cir(AB)}}$, the produced additional dc power can be expressed as follows:

$$\begin{cases} \Delta p_{uA,0}=-\Delta p_{lA,0}=-\sqrt{3}U_oI_{\mathrm{cir(AB)}}\cos(\alpha_1)/2 \\ \Delta p_{uB,0}=-\Delta p_{lB,0}=\sqrt{3}U_oI_{\mathrm{cir(AB)}}\cos(\alpha_2)/2. \end{cases} \tag{14}$$

The definitions of α_1 and α_2 are presented in Fig. 2. Since $\Delta p_{uA,0}=-\Delta p_{uB,0}$, $\alpha_1=\alpha_2$ should be guaranteed. According to the phase angle relationship between u_{AC} and u_{BC} shown in Fig. 2, $i_{\mathrm{cir(AB)}}$ must be in opposite phase with u_{oC} to guarantee $\alpha_1=\alpha_2=\pi/6$. According to (13) and (14), $I_{\mathrm{cir(AB)}}$ is easy to be solved. Finally, the expression of $i_{\mathrm{cir(AB)}}$ is (15). The negative sign means $i_{\mathrm{cir(AB)}}$ is in opposite phase with u_{oC}

$$i_{\mathrm{cir(AB)}}=-(\sqrt{3}I_o\sin\varphi/3)\cos(\omega_o t+2\pi/3). \tag{15}$$

Considering u_{oC} is generally produced by load controllers and $I_{\mathrm{cir(AB)}}$ can be acquired by closed-loop DM energy controllers for different φ, energy balance is much easier to be realized by controlling $i_{\mathrm{cir(AB)}}$ than calculating and controlling $x(\varphi)$ and $k(\varphi)$ in real time. Consequently, the feasible arm current configuration of non-failure arms is as follows:

$$\begin{cases} i_{uA}=-i_{oC}/2+I_{\mathrm{cir}A,0}+i_{\mathrm{cir(AB)}} \\ i_{lA}=-i_{oA}-i_{oC}/2+I_{\mathrm{cir}A,0}+i_{\mathrm{cir(AB)}} \\ i_{uB}=-i_{oC}/2+I_{\mathrm{cir}B,0}-i_{\mathrm{cir(AB)}} \\ i_{lB}=-i_{oB}-i_{oC}/2+I_{\mathrm{cir}B,0}-i_{\mathrm{cir(AB)}} \\ i_{uC}=i_{oC}. \end{cases} \tag{16}$$

Additionally, the actual control objective, i.e., circulating currents, can be further derived as follows:

$$\begin{aligned} i_{\mathrm{cir}A} &= -i_{oA}/2-i_{oC}/2+I_{\mathrm{cir}A,0}+i_{\mathrm{cir(AB)}} \\ i_{\mathrm{cir}B} &= -i_{oB}/2-i_{oC}/2+I_{\mathrm{cir}B,0}-i_{\mathrm{cir(AB)}}. \end{aligned} \tag{17}$$

In conclusion, by configuring arm voltages and arm currents as (4), (5), and (16) [for (4) and (5), u_{com} should be 0], the three essential constraints are all satisfied and the three-phase MMC is capable of operating under the SAF condition.

$$\begin{cases} p_{uA,0}+p_{lA,0}=U_oI_o(-3\cos\varphi-\sqrt{3}\sin\varphi)/4+U_{\mathrm{dc}}I_{\mathrm{cir}A,0}=0,\ p_{uB,0}+p_{lB,0}=U_oI_o(-3\cos\varphi+\sqrt{3}\sin\varphi)/4+U_{\mathrm{dc}}I_{\mathrm{cir}B,0}=0 \\ p_{uA,0}-p_{lA,0}=U_oI_o\left[(-3x+6k)\cos\varphi+\left(2\sqrt{3}-3\sqrt{3}x-2\sqrt{3}k\right)\sin\varphi\right]/4=0 \\ p_{uB,0}-p_{lB,0}=U_oI_o\left[(-3x-6k)\cos\varphi+\left(-2\sqrt{3}+3\sqrt{3}x-2\sqrt{3}k\right)\sin\varphi\right]/4=0 \end{cases} \tag{11}$$

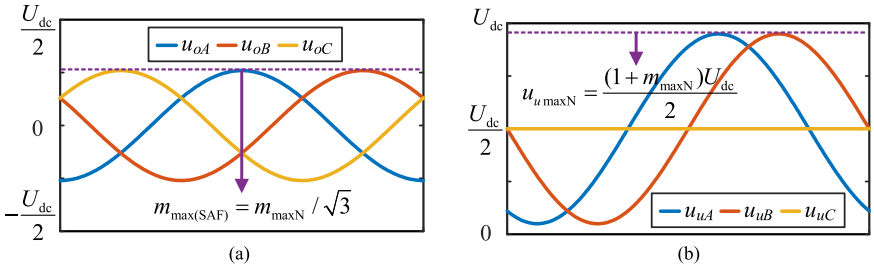

Fig. 3. Limitation of $m_{\max}$ for the HB SM based MMC under the SAF condition when $m_{\max N}$ is 0.9. (a) Original three-phase voltages. (b) Upper arm voltages.

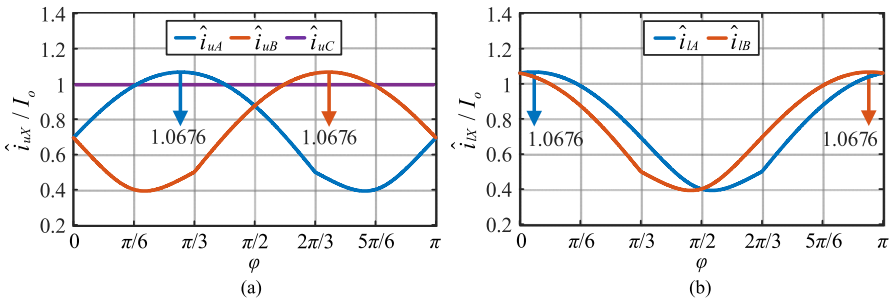

Fig. 4. Normalized peak arm currents under different φ when $m_{\max(\mathrm{SAF})}$ is 0.52. (a) Curves of upper arms. (b) Curves of lower arms.

III. Analysis of Operating Limitations

Although the MMC is capable of operating under the SAF condition by configuring the arm voltage and current as the results in Section II, there are several operating limitations, which are analyzed as follows.

A. Limitation of the Maximum Modulation Index

It can be observed from (5) that the FVCs in the arms of phase A and B change from phase voltage to line voltage, which indicates that the amplitude of FVCs under the SAF condition is $\sqrt{3}$ times larger than that of the normal condition. Consequently, the limitation of $m_{\max}$ needs to be modified. For the half-bridge (HB) SM-based MMC, the limitation of $m_{\max}$ under the SAF condition, $m_{\max(\mathrm{SAF})}$, is illustrated in Fig. 3, with $u_{\mathrm{com}} = 0$. In Fig. 3, $m_{\max N}$ refers to the rated $m_{\max}$ and $u_{u\max N}$ refers to the rated maximum upper arm voltage. According to (5) and the relationship between $m_{\max N}$ and $u_{u\max N}$ shown in Fig. 3(b), $m_{\max(\mathrm{SAF})}$ should be set to $m_{\max N}/\sqrt{3}$ to avoid that u_{uA} and u_{uB} exceed $u_{u\max N}$. For example, if $m_{\max N}$ is set to 0.9 (the value adopted when plotting Fig. 3), $m_{\max(\mathrm{SAF})}$ should be 0.52.

B. Limitation of the Peak Arm Current

According to (11), (15), and (16), the detailed expressions of arm currents can be derived as (18), shown as bottom of this page, where $m_{(\mathrm{SAF})}$ refers to the modulation index under the SAF condition. The first term of each equation is the FCC, and the second term is the dc component. It should be noted that the injection of $i_{\mathrm{cir(AB)}}$ does not influence CMPEs, thus $I_{\mathrm{cir}A,0}$ and $I_{\mathrm{cir}B,0}$ are directly acquired by solving (11). The expressions of β_1 and β_2 are very complex, so they are not presented, which do not influence the analysis of PACs. It is evident that PACs, i.e., $\widehat{i}_{uA}$, $\widehat{i}_{uB}$, and so on, are functions of φ. The curves of them are presented in Fig. 4, with $m_{(\mathrm{SAF})}$ equaling to 0.52, i.e., the value of $m_{\max(\mathrm{SAF})}$ when $m_{\max N}$ is 0.9. From Fig. 4, when φ varies from 0 to π, the maximum PACs of phase A and B are the same, i.e., $1.0676I_o$, while the maximum value of $\widehat{i}_{uC}$ is I_o ($i_{uc} = i_{oc}$). Therefore, the maximum arm current under the SAF condition, $\widehat{i}_{\max(\mathrm{SAF})}$, is $1.0676I_o$

According to [9], if all even-order circulating currents are ignored, the upper arm current under the normal condition is (19), where $m_{(\mathrm{normal})}$ refers to the modulation index under the normal condition. If $m_{(\mathrm{normal})} = m_{\max N} = 0.9$, the maximum arm current under normal condition, $\widehat{i}_{\max(\mathrm{normal})}$, is $0.725I_o$. As a result, $\widehat{i}_{\max(\mathrm{SAF})} = 1.473\widehat{i}_{\max(\mathrm{normal})}$. Therefore, the maximum magnitude of the output current under the SAF condition, $I_{o\max(\mathrm{SAF})}$, should be limited to 67.9% of the rated output current, $I_{o\mathrm{N}}$, if the MMC is desired to operate with any φ

$$i_{uX(\mathrm{normal})} = i_{oX}/2 + m_{(\mathrm{normal})} I_o \cos(\varphi)/4. \tag{19}$$

$$\begin{cases} i_{uA} = \sqrt{1/4 + \sin^2\varphi/3 + \sqrt{3}\sin(2\varphi)/6} \times I_o \cos(\omega t + 2\pi/3 - \beta_1) + \sqrt{3} m_{(\mathrm{SAF})} I_o \cos(\varphi - \pi/6)/4 \\ i_{lA} = -\sqrt{24\cos^2\varphi + 3} \times I_o \cos(\omega t + \pi/6 - \gamma)/6 + \sqrt{3} m_{(\mathrm{SAF})} I_o \cos(\varphi - \pi/6)/4, \gamma = \arctan\left[\tan(\varphi)/3\right] \\ i_{uB} = \sqrt{1/4 + \sin^2\varphi/3 - \sqrt{3}\sin(2\varphi)/6} \times I_o \cos(\omega t + 2\pi/3 - \beta_2) + \sqrt{3} m_{(\mathrm{SAF})} I_o \cos(\varphi + \pi/6)/4 \\ i_{lB} = \sqrt{24\cos^2\varphi + 3} \times I_o \cos(\omega t + \pi/6 - \gamma)/6 + \sqrt{3} m_{(\mathrm{SAF})} I_o \cos(\varphi + \pi/6)/4, \gamma = \arctan\left[\tan(\varphi)/3\right] \end{cases} \tag{18}$$

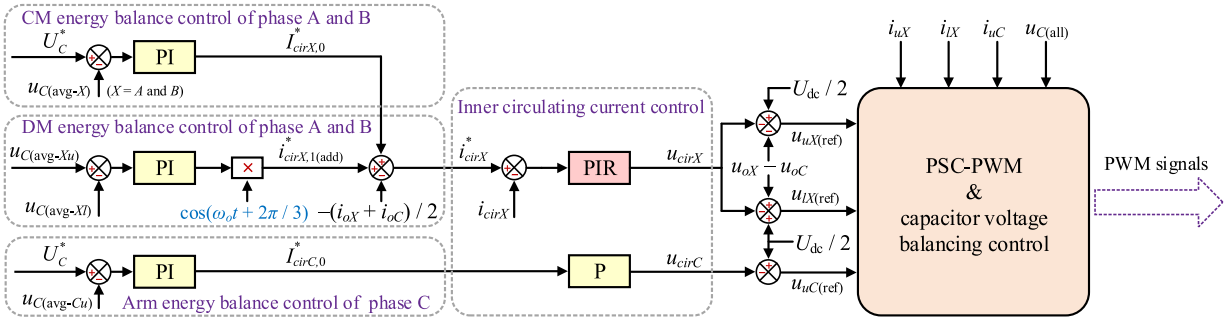

Fig. 5. Control scheme of the MMC when the lower arm of phase C is failed.

C. Limitation of the Capacitor Voltage Fluctuation

If only the CVF caused by the FCC is considered, the magnitude of the CVF, ΔU_C, is in direct proportion to the magnitude of the FCC in each arm. For arms of phase A and B, the maximum magnitudes of the FCC under the SAF condition are all equal to $0.866I_o$, by calculating the maximum value of the FCC in (18) under different φ. While for the upper arm of phase C, that is, I_o, which is the larger one. Considering that each arm supply half of the output current under the normal condition, the maximum magnitude of the FCC under the SAF condition is twice as large as that under the normal condition. Consequently, if the maximum value of ΔU_C under the SAF condition is limited to the same as that under the normal condition, $I_{o\max(\mathrm{SAF})}$ should be further reduced to $0.5I_{o\mathrm{N}}$.

In conclusion, the limitation of $m_{\max}$ determines the maximum output voltage and that of the CVF determines $I_{o\max(\mathrm{SAF})}$. If the configuration of power devices and capacitors are not changed, $m_{\max(\mathrm{SAF})}$ should be limited to $m_{\max\mathrm{N}}/\sqrt{3}$ and $I_{o\max(\mathrm{SAF})}$ should be limited to $0.5I_{o\mathrm{N}}$. As a result, the maximum output power of the arm-fault MMC reduces to 28.9% of its rated value, indicating that it can operate with a light load. If it is desired that the MMC can output rated power under the SAF condition, the number of SMs should be enlarged $\sqrt{3}$ times and the SM capacitance should be enlarged twice.

IV. Control Scheme and Experimental Results

According to the analysis in Section II, the control scheme of the MMC under the SAF condition is presented in Fig. 5, which is similar to the common control scheme utilized in [5]. The CM and DM energy balance control loops are acting as the outer loop controllers to guarantee the energy balance of each arm and generate the reference values of circulating currents. Two key points need to be noted. First, although the DM energy is balanced by injecting $i_{\mathrm{cir(AB)}}$ between phase A and B theoretically, the balancing results may be influenced by circuit-parameter differences in practical systems. Thus, the DM energy balance of phase A and B is independently controlled by $i^*_{\mathrm{cirA},1(\mathrm{add})}$ and $i^*_{\mathrm{cirB},1(\mathrm{add})}$. When circuit-parameter differences are not significant, their summation nearly equals to 0 and "Constraint 3" is still basically satisfied. In addition, for the upper arm of phase C, although its energy is theoretically balanced if i_{uC} and u_{uC} are configured as (2) and (4), the currents flowing through discharge resistors paralleled with SM capacitors still produce dc power and diverge arm energy. Therefore, an arm energy controller is also added to compensate these currents to ensure its energy balance. Considering the discharge currents are quite small, this does not have an evident influence on load currents. Then, the inner loop current controllers are employed to generate the circulating voltages to be injected in arm voltages. Finally, pulsewidth modulation (PWM) signals are generated by phase-shifted carrier (PSC) modulation according to arm voltage references and capacitor voltage balancing control. The common control scheme base on PSC-PWM proposed in [10] is employed to balance the SM capacitor voltages in each arm, which is implemented by adding an individual adjustment to the reference signal of each SM.

TABLE I
Experimental Parameters

Parameters	Value	Parameters	Value
DC-link voltage	$U_{\mathrm{dc}} = 400$ V	Arm inductance	$L = 2$ mH
SMs per arm	$N = 4$	Carrier frequency	$f_{\mathrm{c}} = 2$ kHz
SM capacitance	$C = 4.7$ mF	*R-L* Load	$R_{\mathrm{Load}} = 14\ \Omega$ $L_{\mathrm{Load}} = 10$ mH

To verify the validity of the proposed fault control strategy, a three-phase MMC prototype with four HB SMs per arm is built. The central controller consists of a digital signal processor (DSP) chip TMS320F28335 and a field-programmable gate array (FPGA) chip EP1C12Q240C6. Each SM is controlled by a complex programmable logic device (CPLD) chip EPM570T100C5. The detailed experimental parameters are presented in Table I, an *R–L* load is employed.

Consistent with Fig. 1, the fault of the lower arm in phase C is considered and imitated by connecting a mechanical breaker with it. The arm fault experiment is conducted as follows.

At the very beginning, the MMC prototype operates under the normal condition, with $m_{(\mathrm{normal})} = 0.8$ and the output frequency $f_{o(\mathrm{normal})} = 50$ Hz. When the mechanical breaker is controlled open, all the SMs are blocked and the output voltages equal to 0. After a period of time (1 s), it restarts and operates under the SAF condition, with $m_{(\mathrm{SAF})} = 0.5$ and output frequency $fo_{(SAF)} = 30$ Hz. This experiment process aims to imitate the restart with speed control of the motor when one arm of the MMC is failed. Because for motor drive applications, if the motor operates at the rated speed when an arm fault appears, the output voltage of the HB-based MMC is unable to counteract the back electromagnetic force (EMF) and all the

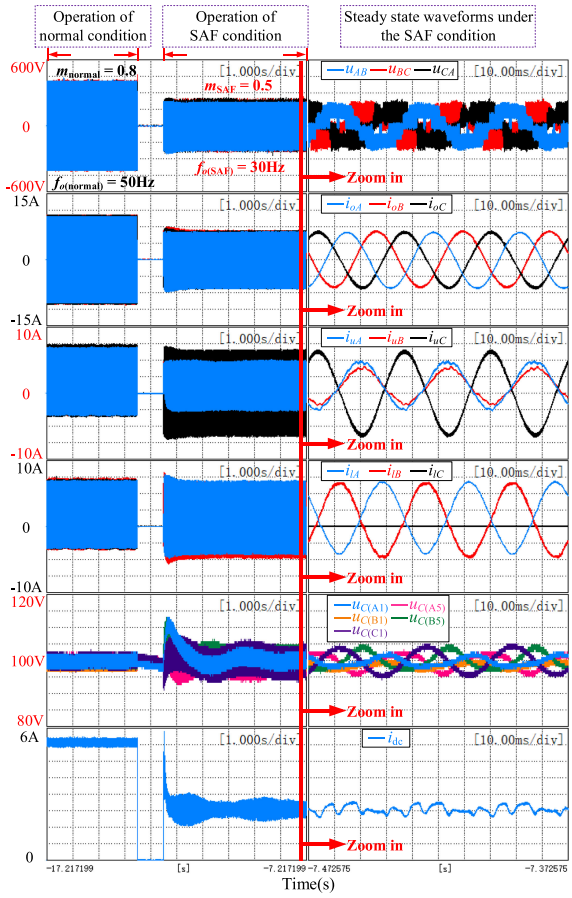

Fig. 6. Experiment results of switching process from normal to SAF condition (left) and steady state of SAF condition (right).

SMs should be blocked to avoid over-modulation, according to the $m_{\max}$ limitation shown in Fig. 3(a). Then, the motor begins to decelerate and its back EMF decreases. When the back EMF decreases to a certain value satisfying the mmax limitation, the MMC can be restarted and drive the motor again, by employing vector control and the proposed fault control method. It should be noted that the motor speed is a little larger than half of its rated value once the back EMF is small enough, according to the voltage-frequency relationship of the motor. Therefore, $fo_{(SAF)}$ is set to 30 Hz under the SAF condition. Moreover, the motor can be accelerated near to its rated speed by flux-weakening control if necessary in practical application.

Fig. 6 shows the experiment result of the switching process from normal to SAF condition and the steady state of the SAF condition. $u_{C(\mathrm{A1})}$ and $u_{C(A5)}$ are the capacitor voltage of No.1 SM (upper arm) and that of No.5 SM (lower arm) in the phase A, respectively, the same as the other two phases. For the steady state of the SAF condition, it is evident that i_{lC} is 0 because the lower arm of phase C is disconnected. The output line voltages and currents are desired values with the frequency equaling to 30 Hz, thus "Constraint 1" is satisfied. For "Constraint 2," the average capacitor voltages of SMs in all non-failure arms are controlled to 100 V, suggesting that the arm energy is balanced admirably. With respect to i_{dc}, although there are a few ripples caused by the asymmetry of each arm and other non-ideal factors, it does not contain significant FCC and "Constraint 3" is still satisfied well. Therefore, the three essential constraints are satisfied and the stable operation of the arm-fault MMC is realized, which can improve the system reliability under such server fault condition. Additionally, the waveforms of arm currents are in accord with (18) and Fig. 4 ($\varphi = 0.149$ rad). ΔU_C of each arm is also in coincidence with the magnitude of the FCC in it. Thus, the analysis in Section III is also verified.

V. Conclusion

In this letter, a control strategy to realize the operation of the MMC under the SAF condition is proposed and verified. According to the three primary constraints of the normally operating MMC, the feasible arm voltage and current configuration under the SAF condition are derived step by step, which proves that it is capable of operating under the SAF condition, with the limited maximum modulation index (57.7% of the rated value) and less power capability (28.9% of the rated value). The SAF operation is verified by experimental results, especially the excellent control results of arm energy balance. In addition, arm currents are also in coincidence with the theoretical analysis. Notwithstanding its limitations, the proposed control strategy can guarantee the operation of the arm-fault MMC under light loads, which is applicable for voltage-variable dc/ac applications, especially motor drive applications with high-reliability requirements. For ac/dc applications, such as gird connection applications, the ac voltage is generally fixed. Therefore, the proposed method is not applicable, unless increasing the number of redundant SMs in the design phase.

References

[1] A. Lesnicar and R. Marquardt, "An innovative modular multilevel converter topology suitable for a wide power range," in *Proc. IEEE Bologna Power Tech Conf.*, Bologna, Italy, 2003, vol. 3, p. 6.

[2] A. Dekka, B. Wu, R. L. Fuentes, M. Perez, and N. R. Zargari, "Evolution of topologies, modeling, control schemes, and applications of modular multilevel converters," *IEEE J. Emerg. Sel. Topics Power Electron.*, vol. 5, no. 4, pp. 1631–1656, Dec. 2017.

[3] W. Zhou, J. Sheng, H. Luo, W. Li, and X. He, "Detection and localization of submodule open-circuit failures for modular multilevel converters with single ring theorem," *IEEE Trans. Power Electron.*, vol. 34, no. 4, pp. 3729–3739, Apr. 2019.

[4] B. Li, S. Shi, B. Wang, G. Wang, W. Wang, and D. Xu, "Fault diagnosis and tolerant control of single IGBT open-circuit failure in modular multilevel converters," *IEEE Trans. Power Electron.*, vol. 31, no. 4, pp. 3165–3176, Apr. 2016.

[5] B. Li, Z. Xu, J. Ding, and D. Xu, "Fault-tolerant control of medium-voltage modular multilevel converters with minimum performance degradation under submodule failures," *IEEE Access*, vol. 6, pp. 11772–11781, 2018.

[6] K. Li, L. Yuan, Z. Zhao, S. Lu, and Y. Zhang, "Fault-tolerant control of MMC with hot reserved submodules based on carrier phase shift modulation," *IEEE Trans. Power Electron.*, vol. 32, no. 9, pp. 6778–6791, Sep. 2017.

[7] D. Karwatzki, M. von Hofen, L. Baruschka, and A. Mertens, "Operation of modular multilevel matrix converters with failed branches," in *Proc. 40th Annu. Conf. IEEE Ind. Electron. Soc.*, Dallas, TX, USA, 2014, pp. 1650–1656.

[8] B. Fan, K. Wang, Z. Zheng, L. Xu, and Y. Li, "Optimized branch current control of modular multilevel matrix converters under branch fault conditions," *IEEE Trans. Power Electron.*, vol. 33, no. 6, pp. 4578–4583, Jun. 2018.

[9] B. Li *et al.*, "An improved circulating current injection method for modular multilevel converters in variable-speed drives," *IEEE Trans. Ind. Electron.*, vol. 63, no. 11, pp. 7215–7225, Nov. 2016.

[10] M. Hagiwara and H. Akagi, "Control and experiment of pulsewidth-modulated modular multilevel converters," *IEEE Trans. Power Electron.*, vol. 24, no. 7, pp. 1737–1746, Jul. 2009.